



**HAL**  
open science

# Investigation of 3D effects and free-surface proximity influence on the flow around a hydrofoil using PIV measurements

H. Bonnard, L. Chatellier, Laurent David

► **To cite this version:**

H. Bonnard, L. Chatellier, Laurent David. Investigation of 3D effects and free-surface proximity influence on the flow around a hydrofoil using PIV measurements. 20th International Symposium on Application of Laser and Imaging Techniques to Fluid Mechanics, Jul 2022, Lisbon, Portugal. hal-03873831

**HAL Id: hal-03873831**

**<https://hal.science/hal-03873831>**

Submitted on 13 Dec 2022

**HAL** is a multi-disciplinary open access archive for the deposit and dissemination of scientific research documents, whether they are published or not. The documents may come from teaching and research institutions in France or abroad, or from public or private research centers.

L'archive ouverte pluridisciplinaire **HAL**, est destinée au dépôt et à la diffusion de documents scientifiques de niveau recherche, publiés ou non, émanant des établissements d'enseignement et de recherche français ou étrangers, des laboratoires publics ou privés.

# Investigation of 3D effects and free-surface proximity influence on the flow around a hydrofoil using PIV measurements

Hervé Bonnard<sup>1,2</sup>, Ludovic Chatellier<sup>1</sup>, Laurent David<sup>1</sup>

<sup>1</sup>Institut P', UPR 3346 CNRS - Université de Poitiers - ISAE-ENSMA

<sup>2</sup>herve.bonnard@univ-poitiers.fr

## 1 Context

Hydrofoils are lifting surfaces which aim to lift a boat out of the water in order to reduce the hull's drag. They aim to improve the boat's performance and are thus very popular in sailing competitions such as the Vendée Globe or the America's Cup. The sections of hydrofoils can be quite different from those of airfoils as they have to be designed with the specific operating conditions of the sea, such as the presence of the free-surface and the risk of cavitation. The latter can be controlled by designing specific hydrofoils shapes which minimize the pressure loss on the suction side. Such profile was for example designed by Eppler and Shen [1] through prescribing a velocity distribution at different angle of attack and using an inverse method based on a combination of a panel method to analyse a potential flow with a boundary-layer method. The study of the influence of free-surface proximity on performance is important for sailing yachts as they are rarely equipped with feedback control loop and thus waves or changes in wind can lead to their foils getting closer to the free-surface.

An Eppler 817 (E817) hydrofoil [2] was studied experimentally using two dimensions two components Particles Image Velocimetry (PIV) measurements. The data were acquired on both an extruded 2D hydrofoil and a 3D "T-shaped" hydrofoil, composed of a vertical shaft (e.g. rudder on a boat) holding the horizontal lifting surface. They were used to investigate the influence of both the 3D shape and surface proximity on the hydrofoil's behaviour. Additional measurements from a 6-axis loads sensor were used to characterize the loss of performance due to the free-surface proximity. Those were also compared to the forces predicted on the 2D profile by various means, such as pressure field reconstruction from PIV, simulations, as well as data-assimilation. The study was done over a range of low chord-based Reynolds numbers  $0.4 \cdot 10^3 \leq Re_c \leq 20 \cdot 10^3$  and four angles of attack  $\alpha = 2^\circ, 6^\circ, 12^\circ, 30^\circ$ .

The first 2D PIV measurements on the extruded profile were done on a large field (about 3.5 chords upstream and downstream of the hydrofoil) at the cost of a coarser resolution, in order to analyse the whole flow, including region with little influence of the hydrofoil. Those data are especially useful in the context of data assimilation for which knowing the upstream conditions is crucial to define the simulation's inlet. The second measurements series were done using time-resolved 2D PIV on a smaller region (length of about 2.5 chords) with a much finer resolution. Meldi and Poux [3] along with Suzuki, Chatellier, Jeon *et al.* [4] highlighted the difficulties of assimilating experimental data due to the limited extent of the physical domain covered by the PIV data as well as the under-sampling of experimental data compared to the time steps of numerical simulations. The two datasets acquired will thus be used to investigate the effect of these parameters on different flows topologies and dynamics.

## 2 Experimental setup

The experiments were carried out at the P' Institute in the Environmental Hydrodynamic Platform's open water channel (see 1) which dimensions are  $7 \text{ m} \times 0.385 \text{ m} \times 0.6 \text{ m}$  (LxWxH). The channel is equipped with a PCM Moineau worm-drive pump controlled with a Schneider Electric variable-frequency drive up to flow rates of  $Q = 65 \text{ L s}^{-1}$ . The flow rates are measured with an Endress+Hauser Promag55 electromagnetic flow-meter. The free-surface height can be modified by a spillway gate.

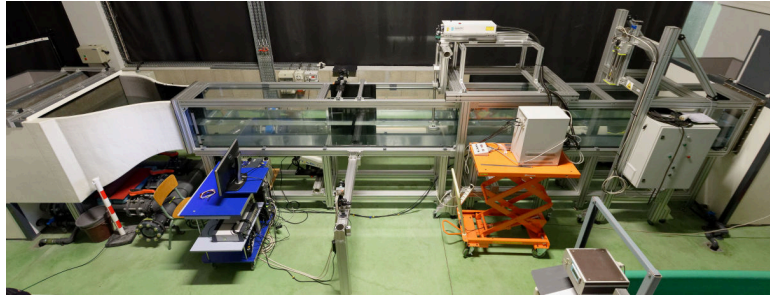
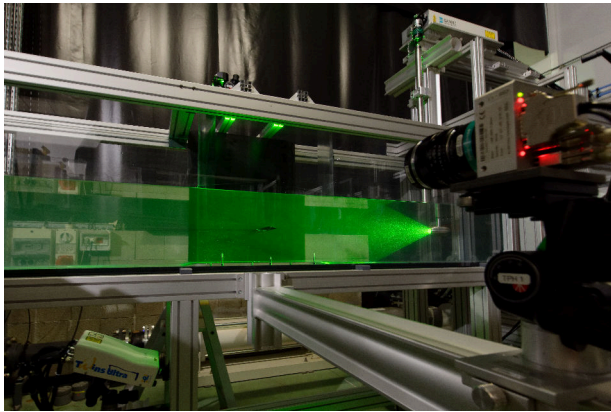
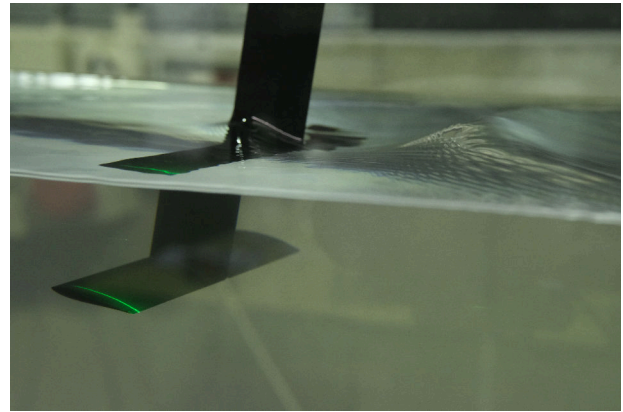


Figure 1: Overview of the water channel with wing model support and PIV setup.



(a) Extruded 2D hydrofoil



(b) 3D "T-shaped" hydrofoil

Figure 2: Photographs of the experimental setups

For the 2D study, the extruded hydrofoil of chord  $c = 40$  mm and span  $s = 355$  mm was placed in the middle of the water volume such as the distance between the profile and either the free-surface or the bottom wall was 3.5 chords. A first series of 2D PIV measurements was carried out using a Dantec SpeedSense 1040 4 MP 100 Hz camera on 16 cases (4 Reynolds numbers and 4 angles of attack). As an opaque 3D-printed ABS hydrofoil was used, two lasers were required in order to get the largest illumination. A  $2 \times 30$  mJ Nd:YAG Quantel Twins Ultra (532 nm, 20 Hz) was placed below the water channel to illuminate the pressure side of the foil as well as the upstream flow. The free-surface of the open water tunnel prevent the use of a laser from the top of the experiment, thus a  $2 \times 50$  mJ Nd:YAG Litron Nano L 50-50 PIV (532 nm, 50 Hz) was used with LaVision underwater illumination unit in order to view the suction side of the foil and the downstream flow. The measurement equipments are depicted on Figure 2a. For each case, 1000 double-frame images were acquired at a very low frequency (2 Hz to 5 Hz) in order to provide statistically relevant datasets.

Then a second series of 2D PIV measurements was done using a Vision Research Phantom VEO 4K 990L 8 MP 1 kHz camera on 12 cases (same cases as the previous one without the lowest Reynolds number). A  $2 \times 30$  mJ Nd-YLF Continuum Terra PIV (527 nm, 10 kHz) was also used downstream with LaVision underwater illumination unit. As a single laser was used, the upstream part of the flow was hidden by the hydrofoil's shade for those measurements. Time-Resolved PIV (TR-PIV) series of 5 000 images were acquired for which a multi-frame PIV method was applied to evaluate the time resolved flow fields using a Fluid Trajectory Evaluation based on an Ensemble-averaged cross-correlation (FTTE) technique [5]. This second dataset complements the first one, as it provides an understanding of both the global mean flow and the dynamics of the flow fluctuations near the hydrofoil.

For the 3D study on the T-shaped hydrofoil (chord  $c = 40$  mm and span  $s = 200$  mm), the depth of the main (horizontal) part of the hydrofoil was set to 3.5 chords, 1.75 chords or 0.875 chords in order to observe the influence of the proximity to the free-surface on the flow. For each depth, measurements were done on three positions on the half-span of the hydrofoil:

- symmetry plane of the hydrofoil

- the middle of the half-span
- 4 mm (0.1 chord or 0.02 span) from the wing tip

Cases were limited to angles of attack  $\alpha = 6^\circ$  and  $12^\circ$  at the two highest chord-based Reynolds number  $Re_c = 6300$  and  $20000$ . The depth based Froude number  $Fr_d$  thus ranged from 0.13 to 0.83. The hydrofoil and the laser sheet near the wing tip are illustrated on the Figure 2b. In addition, force measurements were acquired using a 6-axis load sensor ATI Nano17 IP68 (calibration SI-25-0.25, resolution of 1/160 N and 1/32 Nmm). The loads were mainly used to calculate the lift and drag coefficients of the hydrofoil in order to estimate its performance. Those data allowed us to investigate both 3D effects due to the presence of the wing tip and the vertical shaft, as well as the influence of the proximity to the free-surface on the performance.

### 3 Initial results

#### 3.1 Extruded 2D hydrofoil

Different types of vortex shedding can be observed around a lifting surface: attached flow, trailing edge vortex, separation vortex, leading edge vortex and bluff-body effects [6]. The former were not observed on our hydrofoil as they need extreme angles of attack which do not occur during normal operating conditions. The data from the extruded 2D hydrofoil were used to determine which kind of vortex shedding occurred for our cases. An analysis was based on statistical data such as the standard deviation of the vertical velocities, which highlights the area where vortices are present. An example is showed on Figure 3 with the transition from attached flow to trailing edge vortices at an angle of attack  $\alpha = 2^\circ$ . The transition is showed through the more important fluctuations of the vertical velocities in the wake, which are characteristic of vortex shedding. Such observations were validated by comparison to the time-resolved PIV measurements done on a smaller zone near the hydrofoil. A snapshot of the velocity fields from the case showed on Figure 3 can be found on figure 4, which confirms the apparition of the first vortex shedding for the biggest of the two chord-based Reynolds number represented. The different vortex shedding modes observed in our parameter space are represented by the cartography from Figure 5.

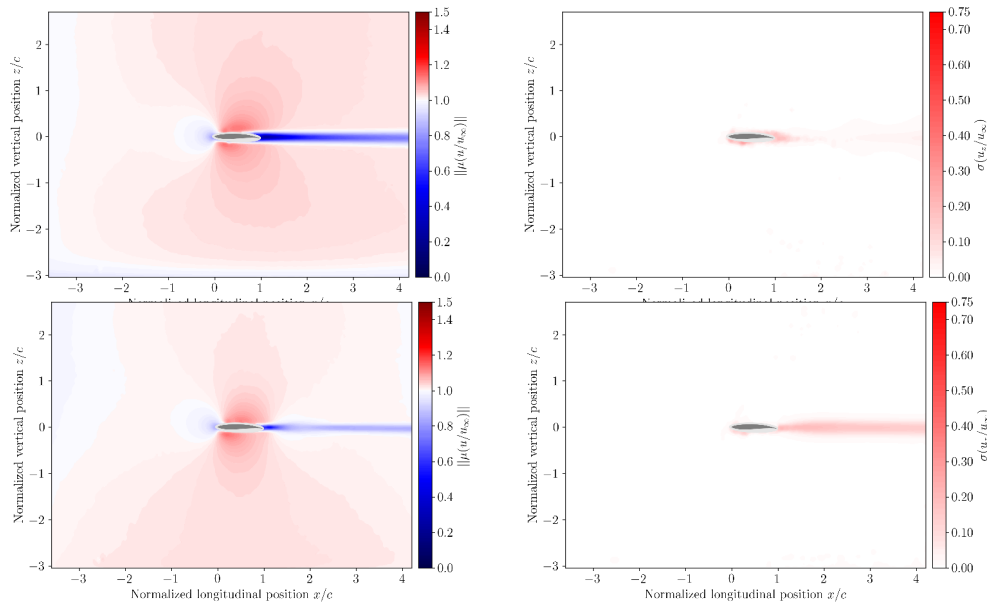


Figure 3: Mean normalized velocities (left) and standard deviation of normalized vertical velocities (right) at  $\alpha = 2^\circ$  for  $Re_c = 1400$  and  $6300$  (rows). The hydrofoil is represented as a dark grey area and the light grey mask corresponds to a zone where data could not be obtained accurately.

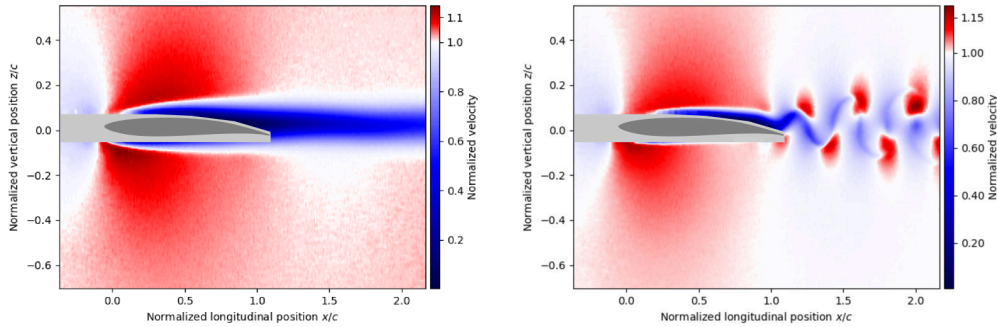


Figure 4: Instantaneous velocity field at  $\alpha = 2^\circ$  for  $Re_c = 1400$  and  $6300$  (left and right). The hydrofoil is represented as a dark grey area and the light grey mask corresponds to a zone where data could not be obtained accurately.

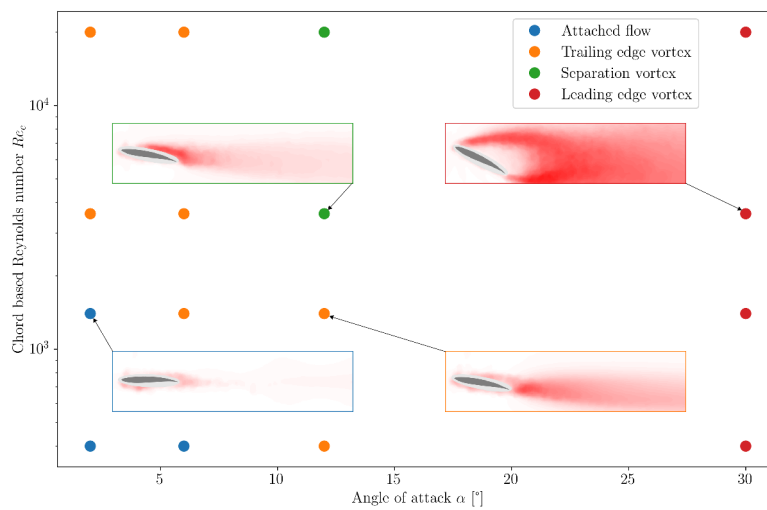


Figure 5: Flows modes observed on our Eppler 817 hydrofoil as a function of chord based Reynolds number  $Re_c$  and angle of attack  $\alpha$ . A zoom of the standard deviation of the vertical velocity graphs was added at some points to illustrate the differences between the modes.

### 3.2 3D "T-shaped" hydrofoil

The 2D two components PIV as well as our forces measurements on the 3D "T-shaped" hydrofoil allowed us to investigate both 3D effects due to the presence of the wing tip and the vertical shaft, as well as the influence of the proximity to the free-surface on the performance. A comparison between the flow around the 2D hydrofoil and near the wing tip of the 3D hydrofoils at two different depths is shown on Figure 6 for an angle of attack  $\alpha = 12^\circ$  and Reynolds number  $Re_c = 20000$ . The two first columns show the influence of the wing tip on the velocity field. We observe a transition from a separated flow on the 2D hydrofoil to trailing edge vortices near the wing tip. This is a consequence of the downward flow caused by the finite span of the wing, which reduces the effective angle of attack of the hydrofoil near the tip [7]. Besides the trailing edge vortices' wake, a second one can be seen due to the wing tip vortices folding inward. A comparison between the two latest columns of the figure, that is the 3D hydrofoil at an important and low depths, shows how the free-surface proximity affect the flow. The first difference can be seen through the standard deviation of the velocity, where the wake is bent for the case closest to the free-surface. The second difference is a lower velocity near the suction side of the hydrofoil and thus a smaller velocity gradient near the leading edge. This is the most important difference as this translate to a lower loss of pressure on the suction side which leads to a lower lift. Those observations were confirmed by the results obtained on the 6-axis load sensor, as can be seen with the Figure 7, which shows the lift coefficient polar at the three depths and highlights the loss of lift when the hydrofoil gets closer to the free-surface.

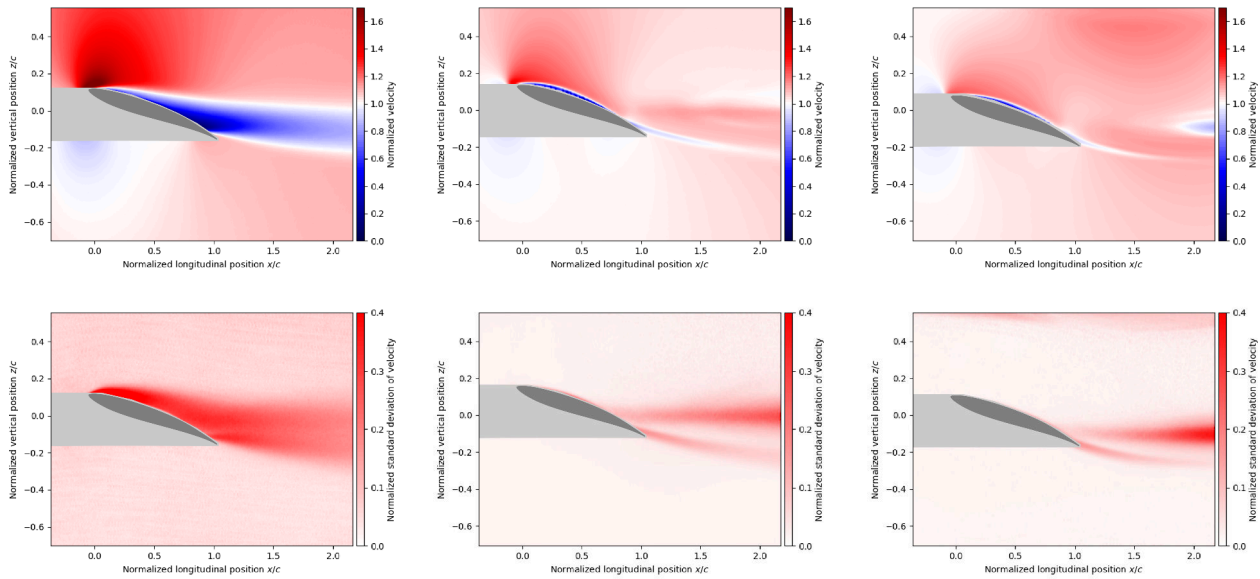


Figure 6: Mean velocity field and standard deviation of the velocity (top and bottom) at  $\alpha = 12^\circ$  for  $Re_c = 20000$  of the 2D hydrofoil (left) and near the wing tip of the 3D hydrofoil at an important depth  $= 3.5 * c$ ,  $Fr_d = 0.42$  (centre) and at a low depth  $= 0.875 * c$ ,  $Fr_d = 0.83$ . The hydrofoil is represented as a dark grey area and the light grey mask corresponds to a zone where data could not be obtained accurately.

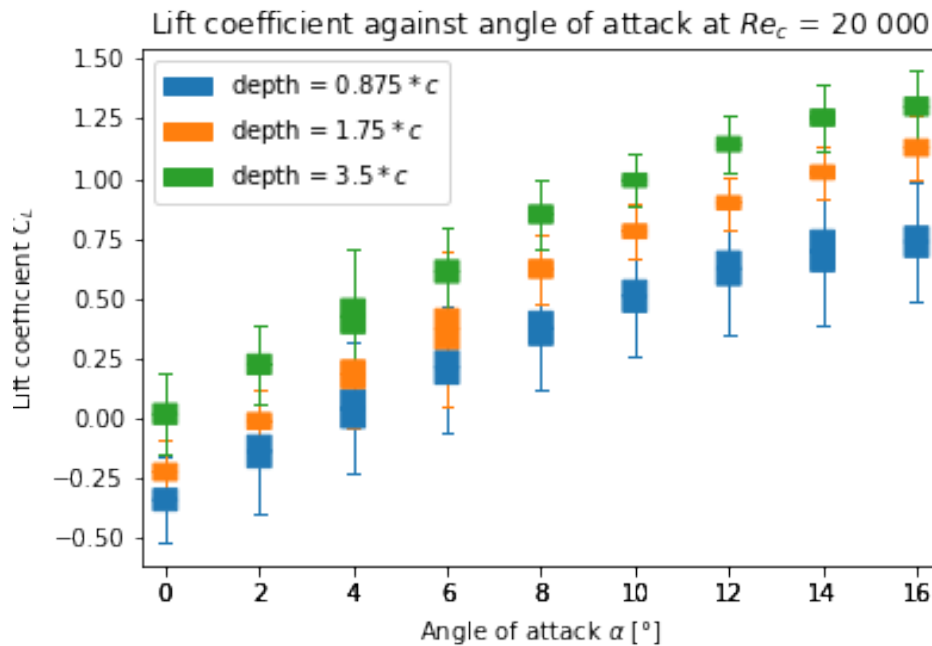


Figure 7: Box plots of lift coefficients measured with the loads sensor as a function of the angle of attack  $\alpha$  and depth.

## Acknowledgments

The authors would like to thank the Direction Générale de l'Armement for the funding of Hervé Bonnard's PhD thesis as well as the Plateforme Hydrodynamique Environnementale (PHE) from the Université de Poitiers which provided the open water channel used for the experiments.

## References

- [1] R. Eppler and Y. T. Shen, 'Wing Sections for Hydrofoils—Part 1: Symmetrical Profiles,' *Journal of Ship Research*, vol. 23, no. 03, pp. 209–217, 1st Sep. 1979. DOI: [10.5957/jsr.1979.23.3.209](https://doi.org/10.5957/jsr.1979.23.3.209).
- [2] R. Eppler, *Airfoil Design and Data*. Berlin, Heidelberg: Springer Berlin Heidelberg, 1990, ISBN: 978-3-662-02648-9 978-3-662-02646-5. DOI: [10.1007/978-3-662-02646-5](https://doi.org/10.1007/978-3-662-02646-5).
- [3] M. Meldi and A. Poux, 'A reduced order model based on Kalman filtering for sequential data assimilation of turbulent flows,' *Journal of Computational Physics*, vol. 347, pp. 207–234, Oct. 2017. DOI: [10.1016/j.jcp.2017.06.042](https://doi.org/10.1016/j.jcp.2017.06.042).
- [4] T. Suzuki, L. Chatellier, Y. J. Jeon and L. David, 'Unsteady pressure estimation and compensation capabilities of the hybrid simulation combining PIV and DNS,' *Measurement Science and Technology*, vol. 29, no. 12, p. 125 305, 1st Dec. 2018. DOI: [10.1088/1361-6501/aae6b7](https://doi.org/10.1088/1361-6501/aae6b7).
- [5] Y. J. Jeon, L. Chatellier and L. David, 'Fluid trajectory evaluation based on an ensemble-averaged cross-correlation in time-resolved PIV,' *Experiments in Fluids*, vol. 55, no. 7, p. 1766, Jul. 2014. DOI: [10.1007/s00348-014-1766-9](https://doi.org/10.1007/s00348-014-1766-9).
- [6] R. F. Huang, J. Y. Wu, J. H. Jeng and R. C. Chen, 'Surface flow and vortex shedding of an impulsively started wing,' *Journal of Fluid Mechanics*, vol. 441, pp. 265–292, 25th Aug. 2001. DOI: [10.1017/S002211200100489X](https://doi.org/10.1017/S002211200100489X).
- [7] A. F. Molland and S. R. Turnock, 'Physics of control surface operation,' in *Marine Rudders and Control Surfaces*, Elsevier, 2007, pp. 21–56, ISBN: 978-0-7506-6944-3. DOI: [10.1016/B978-075066944-3/50006-8](https://doi.org/10.1016/B978-075066944-3/50006-8).